Fluctuations of Broadband Acoustic Signals in Shallow Water

Mohsen Badiey
College of Earth, Ocean, and Environment
University of Delaware
Newark, DE 19716
Phone: (302) 831-3687 Fax: (302) 831-3302 Email: badiey@udel.edu

Award Number: N00014-13-1-0306
http://oalab.cms.udel.edu

LONG-TERM GOALS

The long-term goal of this project is to obtain quantitative understanding of the physical mechanisms governing broadband (50 Hz to 50 kHz) acoustic propagation, reflection, refraction, and scattering in shallow water and coastal regions in the presence of temporal and spatial ocean variability.

OBJECTIVES

The scientific objective of this research is to understand acoustic wave propagation in a dynamic environment in two frequency bands: Low (50 Hz to 500 Hz) and Mid-to-High (500 Hz to 50 kHz). The goal for the low frequency band is to assess the effects of internal waves on acoustic wave propagation, with an emphasis on the mechanisms that cause significant temporal and spatial acoustic fluctuations. The goal for the mid-to-high frequency band is to assess the effects of water column and dynamic sea surface variability, as well as source/receiver motion on acoustic wave propagation for underwater acoustic communications, tomography, and other applications.

APPROACH

The project combines theoretical, experimental, and modeling efforts to improve our understanding of broadband acoustic wave propagation in a dynamic shallow water environment. Studies in the low frequency band have been focused on the data from the SW06 experiment for acoustic sources with vertical and horizontal array receivers. A 3D acoustic propagation model has been utilized and a detailed 3D environment data required as input to the model has been constructed using temperature and radar image data. Improvement has been made with better estimation of the internal wave front location and better understanding of the temporal and spatial coherence of sound propagation.

Studies in the mid-to-high frequency band have utilized data collected at KAM08 [1] and KAM11 [2] experiments. The effects of sea surface, including surface bubbles, and water column variability on acoustic wave propagation have been investigated using Parabolic Equation (PE) model and multiple raytracing models. A time evolving nonlinear sea surface wave model is being developed to realistically simulate the sea surface and wave breaking to determine the location of surface bubbles generation. To take into account the out-of-plane acoustic scattering and the directionality of the surface wave, the PE acoustic propagation model is being extended to 3D.

WORK COMPLETED

1) Low Frequency Acoustic Wave Propagation

A detailed 3D environment, reconstructed based on shipboard radar images and temperature data [3], are developed to study acoustic propagation scenario with vertical and horizontal array receivers in the presence of internal waves. Through modal decomposition at the vertical array, acoustic modes were identified at the horizontal array. Strong refraction of multiple modes were observed for before, onset, and within the interval wave presence. The acoustic refraction created either uneven distribution of modal energy over the horizontal array or additional returns observable at the entire L-shape array. Acoustic ray-mode simulations are provided to explain the observed modal behaviors.

2) *Mid-to-High Frequency Acoustic Wave Propagation*

We have continued our analyses of data from KAM08 and KAM11 to assess the effects of the environment on the acoustic wave propagation. For modeling, time-evolving rough sea surfaces used as boundaries in the PE model were re-generated using waverider buoy data from KAM08 and KAM11. A rough surface model was used from our previous results [4,5] and developed and included in the BELLHOP Ray model to study the effects of surface roughness on acoustic propagation. Results from surface wave acoustic stiration patterns in form of arrival times from the Ray model compared well with data and specific features relevant to the acoustic communication research are being studied in detail. Additional study has been conducted on short time scale fluctuations in acoustic intensity using beamforming on direct path and bottom bounce signals.

RESULTS

A. Low Frequency Acoustic Wave Propagation in the Presence of Shallow Water Internal Waves

During the SW06 experiment, the water column temperature profile was monitored through a large number of thermistor strings during transmissions of a number of acoustic sources in a shallow water region. Here we examine the acoustic transmission from the Miami Sound Machine (MSM) and reception recorded at the SHARK L-shape array. The water depth was about 79 m at the SHARK array. The acoustic source and receiver array were deployed at the mooring positions #45 and #54, respectively. As shown in Fig.1, the temperature profile showed spatial and temporal variability due to the presence of internal waves (IWs). The three images in Fig. 1 show the temperature profile evolution over time at the source position (#45), middle-way (#32), and receiver (#54) positions from 20:00 to 23:00 on August 17, 2006. Through the use of a three-dimensional mapping technique, the temperature field of the IW was reconstructed by interpolating temperature data at the source, middle-way, and receiver positions. The resulting IW fronts were connected by the fourth order polynomial fitting (see the subplots at the bottom row of Fig. 1).

M-sequences at multiple acoustic frequencies were transmitted from the MSM. The source depth was 56 m. Here we processed the M-sequence centered at the frequency of 101.7253 Hz. The symbol rate of the 63-digit M-sequence was a quarter of the center frequency, about 25 Hz. The nominal bandwidth of the signal, thus, was 25 Hz. The 63-digit M-sequence repeated itself every 2.48 seconds. The total M-sequence duration was 89.18 seconds. The source level was 186 dB re 1 μPa.

The SHARK array had 16 elements as its vertical component distributed over the water column and 32 elements at its horizontal component laid at the seafloor. The vertical line array covered the water

column from 13.5 m to 77.25 m, with uneven element spacing. Its horizontal line array started its first element at 3 m, extended northward, and ended the last element at 468 m, away from the anchor of vertical line array. The horizontal element spacing was 15 m. The horizontal line array and the acoustic track formed an angle of 24 degree, with the MSM located at the eastern side. The received signals from the SHARK array, both its vertical and horizontal elements, were transformed to the baseband at the array sampling rate of 9765.625 Hz.

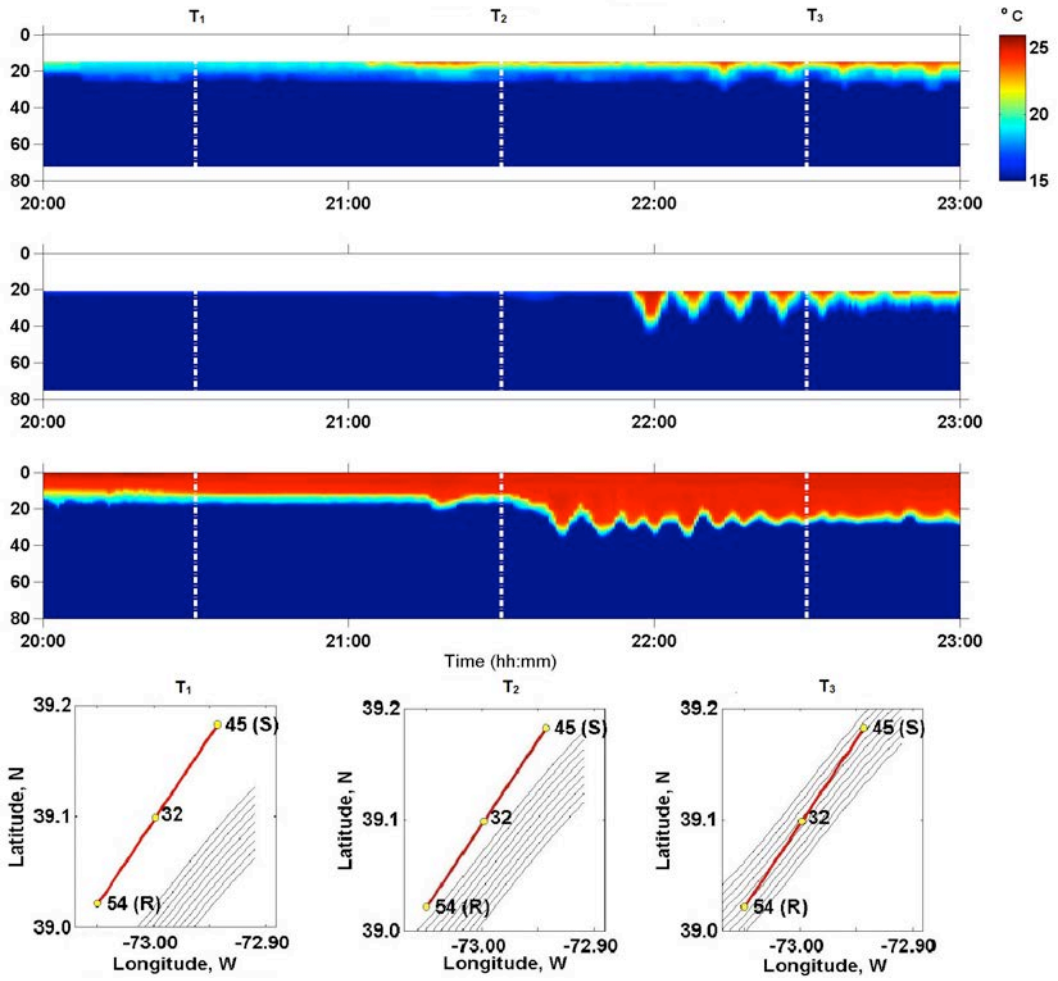

Fig.1. Top panel: Measured temperature profiles as a function of geo-time at the source position (#45), middle point (#32), and Shark receiver position \#54). No temperature measurements in the upper water column at #45 and\#32. T1 (20:30:00), T2 (21:30:00) and T3 (22:30:00) are three different geo-times used in this paper. The white vertical dashed dotted lines indicate the three different geo-times. Bottom panel: Internal wave fronts (black curves) obtained by matching the internal wave propagation at three ocean patches (#54,#32, and #45) within the SW06 experimental area. The acoustic source and receivers were deployed at positions #45 and #54 respectively; the red line marks the acoustic propagation track.

1. Evolution of acoustic modes at the horizontal array in the presence of interval waves

Acoustic modal behaviors were reported at an L-shape hydrophone array when a strong internal wave packet passed through the acoustic source-receiver during the Shallow Water 2006 experiment. Three geo-times, marked as T_1, T_2, and T_3 in Fig.1, are selected to investigate the acoustic normal mode fluctuations for before, onset, and within the internal wave presence. The three subplots at the bottom row of Fig. 1 show the reconstructed internal wave fronts, indicated by multiple parallel curves, at

three forementioned geo-times. Figure 2 shows the evolution of acoustic modal behaviors, when the packet of strong internal waves passed through the acoustic track. In addition to the aforementioned three geotimes, another geo-time (T_0, 06:00:00 GMT on August 11) is chosen to show the modal structure in a quiescent environment, which have no major water column perturbations. In Fig. 2, the top row shows the modal decomposition results for four geotimes T_0-T_3. The first three modes were identified using the reduced rank pseudo-inverse mode filter. The second and third rows show the impulse responses at the vertical and horizontal line arrays, respectively, obtained by the least squares method. In Fig. 2, the middle panel shows the impulse responses at the vertical line array, with the shallowest element shown at the top. The bottom panel shows the impulse responses at the horizontal array, with the furthest element away the vertical line array shown at the bottom. The color indicates the intensity, with the same scale for all the plots. Based on the horizontal line array element positions, the impulse responses at the horizontal line array were shifted by their arrival time differences with the vertical line array. This was to identify the modal structure on the horizontal line array. As shown in Fig. 2, variations of the relative modal arrival times across the horizontal line array was small. This justifies the use of vertical model structure to identify the individual modes across the horizontal line array.

During the quiescent environment at geo-time T_0, three modes are well separated, as shown by the modal decomposition results in the top panel. The three modes have decreasing amplitudes along the mode index. Such mode separation is clearly shown at both the vertical and horizontal line arrays. Prior to the arrival of the strong internal waves at geotime T_1, multiple modal features can be observed. In the modal decomposition subplot, the second mode gets relatively weaker and closer to the first mode than during the quiescent environment. At the horizontal line array, the first two modes basically overlap with each other. Interestingly, the third mode nearly disappears at the second half of the horizontal line array (away from the vertical line array). The disappearance of the third mode on part of the horizontal line array deserves further investigations. A possible explanation is that there is a local scale fluctuations in the water column, prior to the strong internal waves. At geotime T_2, the leading front of the internal wave packet comes close to the acoustic track as shown in Fig.1, bottom-center subplot. The observed acoustic modal features continue their trends. The second mode gets even weaker. Multiple returns show up for the second mode, as shown in the top panel. The first return of the second mode overlaps the first mode. The third mode extends width in the arrival axis, likely as a result of multiple returns, shown in the modal decomposition subplot. At the horizontal line array, additional returns from the second and third modes are shown. Interestingly again, all of the returns from the second and third modes can only be observed at the first half of the horizontal line array. At geotime T_3, when the internal wave packet completely covers the entire source-receiver track, the first two modes collapse into a single return. As shown at the top subplot, the amplitude of the first mode drops significantly. The second mode becomes the strongest. At the horizontal line array, only one strong, focused return appears as the combination from the first two modes.

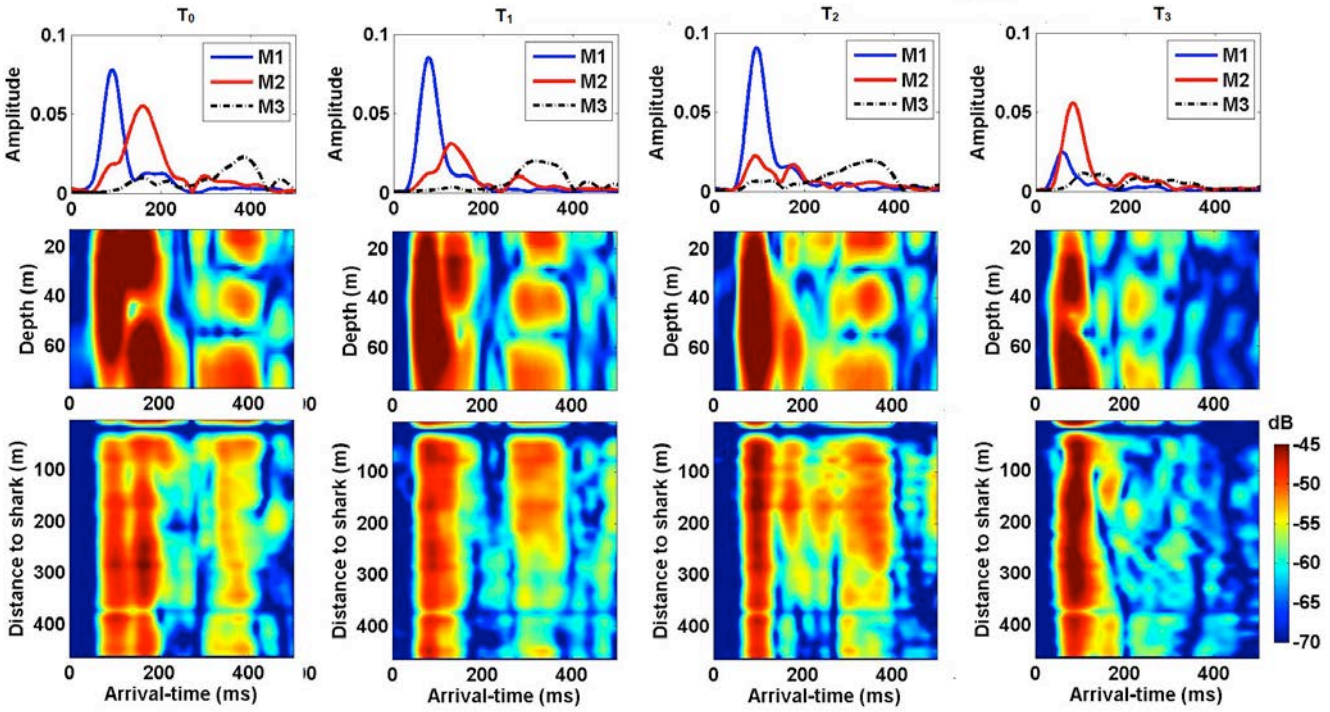

Fig.2. First row: mode decomposition of impulse response of received MSM100 signal. Second and third rows: received impulse response on the vertical line array and the horizontal line array of Shark, respectively.

Multiple features of the modal fluctuations are shown at the horizontal line array in the interval wave field: mainly including 1) multiple returns for the second and third modes and 2) drastic reduction of the relative arrival time for the third mode. Mechanism of both behaviors can be illustrated by the acoustic ray-mode simulations, as shown in Fig. 3. The SW06 source-receiver geometry and SHARK array configuration were adopted. The numerical simulations used a water depth of 78 m and a flat seafloor. A packet of interval waves were simulated to perturb the water column. In the ray subplots at the first column of Fig.3, a circle, marked as R, indicates the vertical line array anchor position. The thick blue line shows the position of the horizontal line array. Multiple red lines indicate the wave fronts of the internal waves. These internal waves have a straight line wave front, approaching the acoustic track at a small angle of 5^{o}.

In Fig.3, the first column shows the ray plots for the first three modes, when the leading wave front just passes position R, the vertical line array anchor position. Due to the presence of the internal waves, i.e., warmer water, the three modes show refraction at the horizontal plane, but at different extents. The first mode shows some degree of ray bending, around the internal wave fronts. However, refraction can barely be observed at the horizontal line array, which is not yet covered by the incoming internal waves. The second mode shows stronger refraction around the internal wave front and minimum refraction at the horizontal line array. Compared with the first two modes, the third mode shows drastic effects of the refraction. A large portion of the rays reflects off the leading internal waves. Only a small portion of the third mode rays penetrate and refract between the two edges of the internal waves. Additional third mode rays appear at the horizontal line array, due to the strong refraction and reflection induced by the internal waves. Multiple refracted and reflected rays indicate possible interference among them. The second column of Fig.3 shows the arrival time fluctuations for the first three modes, observed at position R, when the internal waves pass through the acoustic track. The three rows show the results for the three modes, respectively. In each of the subplots, the horizontal axis represents the relative arrival time in milliseconds. The vertical axis shows the geotime in

minutes, during which the internal waves pass through the region. Overall, the modal arrival time fluctuations show strong variation across the modes. In the simulation, the first mode shows small arrival time fluctuations in several milliseconds. The second and third modes show much larger fluctuations, up to 50 ms for the third mode. In addition, at position R, multiple returns are simulated for all the three modes. However, only the second and third modes have significant separation, in tens of milliseconds.

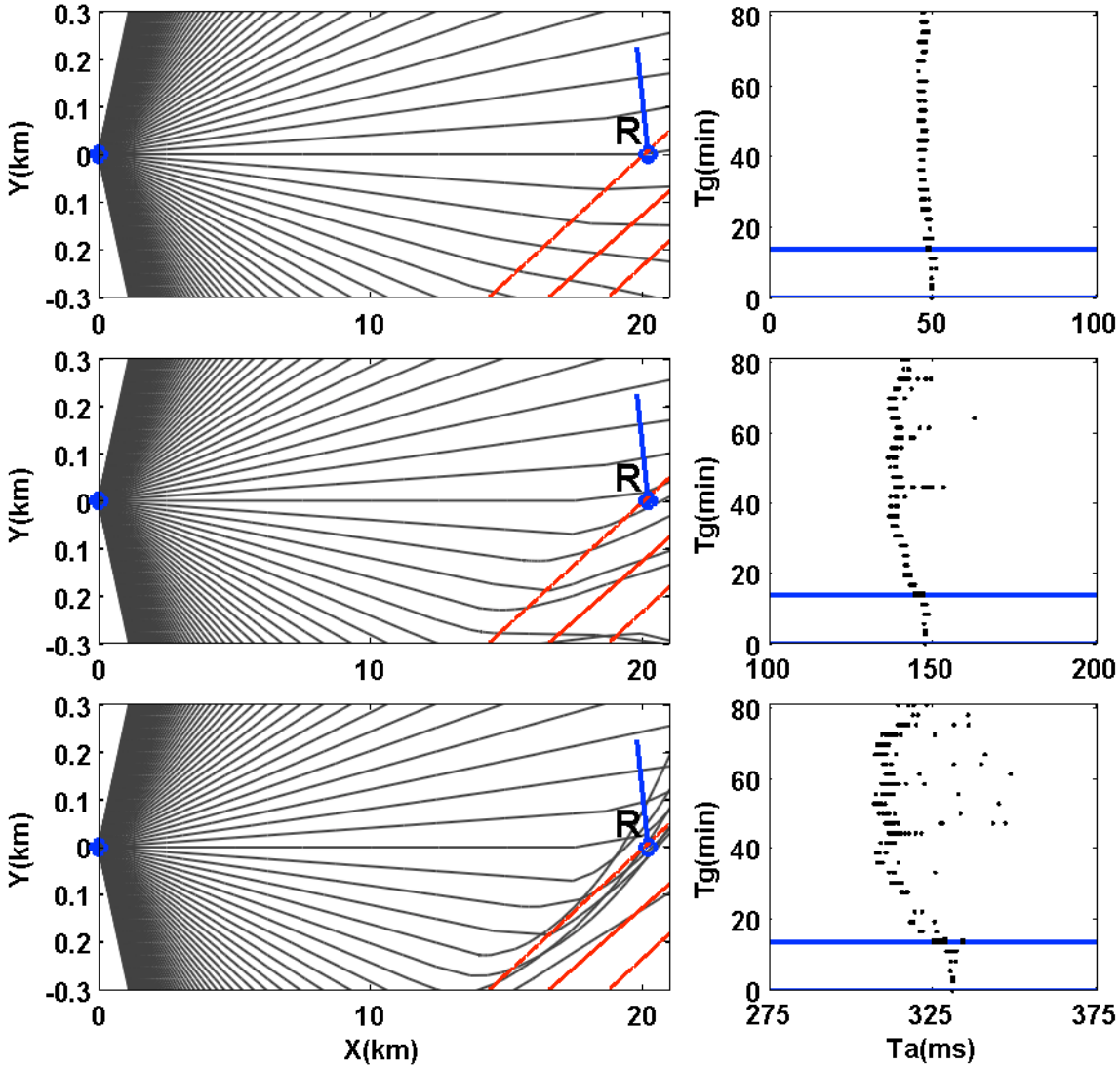

Fig.3. Left panel: Horizontal ray plot showing the effects of the incoming internal wave front on the propagation of vertical modes 1-3 (from top to bottom). The center of the receiver array (marked with a "R" in the figure) indicates the location of the vertical leg of the array with the horizontal leg extended upwards. Two dash lines shows the front and back edges of the internal wave and the dotted line shows its center. The rays of Mode 1 shows little bending by the internal wave, while the rays of mode 2 and 3 are clearly bent and concentrated, which are shown on the received signal plot as multiple arrivals and intensified at the first half of the HLA. Right panel: Geo-time as a function of arrival time of the first three modes (from top to bottom). Two horizontal blue lines in each subplot indicate the geo-times without (lower) and with IW (upper), respectively.

2. Horizontal coherence measurements of normal modes during SW06

The knowledge of spatial coherence of sound field is required for sonar application and array design. In shallow water waveguides, the spatial and temporal evolution of the temperature field induced by internal waves will cause signal fluctuations and variations in spatial coherence. During the Shallow Water Acoustic Experiment 2006, the three dimensional temperature field of internal waves was measured and reconstructed while acoustic signals were simultaneously transmitted between various sources and an L-array. These internal wave events have been used to investigate the internal wave effect on temporal coherence and vertical structures of acoustic normal modes [6]. In this research, the horizontal structures of acoustic normal modes are examined. Figure 4 shows the horizontal coherence of individual normal mode obtained before, onset, and after the IW events during SW 06' experiment.

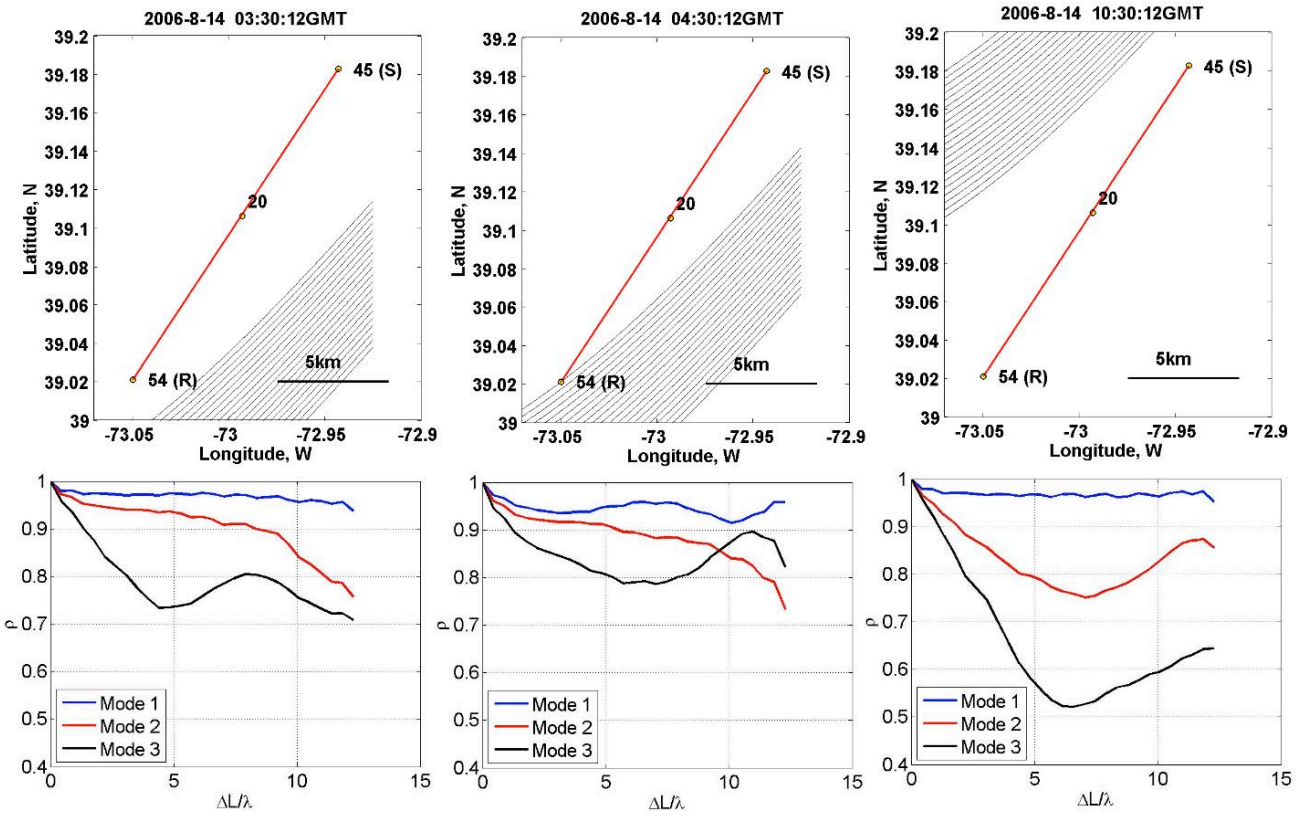

Fig. 4. The picture collage is the example showing the evolution of NLIW event 37 (first row) and the corresponding horizontal coherence of normal modes at 100Hz (second row).

B. Mid-to-High Frequency Acoustic Propagation in Shallow Water

The environment in a recent experiment (KAM11) exhibited short time scale isotherm depressions and elevations in the temperature profile of the water column. This dynamic behavior is significantly pronounced over a 2 hour period (between 70-90 m depth) during a 24 hour deployment. High frequency broadband transmissions (22-28 kHz) were sent between a stationary source (5 m above the seafloor) and an 8-element vertical hydrophone array (4.5 m above the seafloor) in an approximate depth of 100 m with 1 km separation (Figure 5). Vertical beamforming of measured impulse response across all array elements and application of Gaussian steering revealed strong correlation between vertical temperature profiles and angular spread of the direct path receptions (Figure 6). Inherently a 3D problem, we consider a 2D approach to show beam fluctuations as a function of the environment. 2D PE modeling is driven by measured sound speed profiles to calculate the acoustic field between source and receiver and to beamform across an ideal vertical array for data/model comparison. Over time, fluctuations in the intensity of the acoustic beam, spatial path and angular spread of the direct path signal can be attributed to the vertical oscillations of isotherms in the water column.

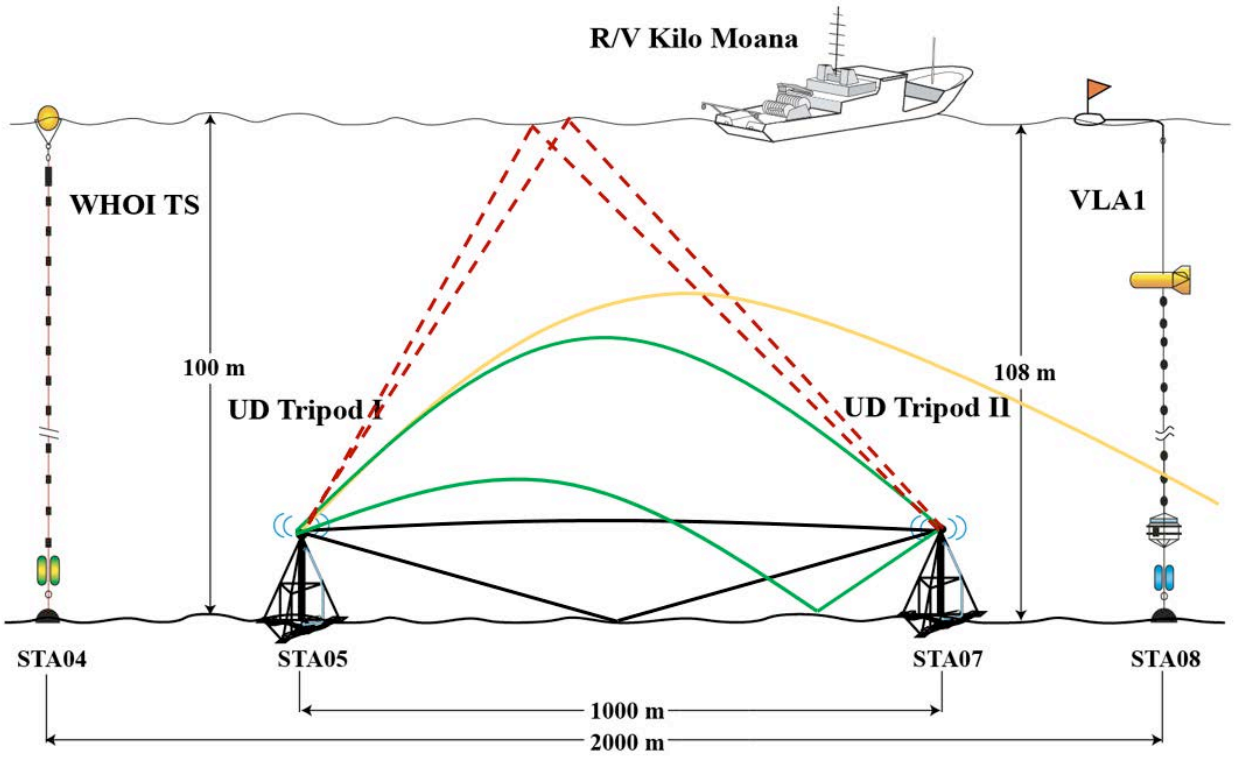

Figure 5. Experimental set-up during the 3rd tripod deployment (07/06 02:00 to 07/07 02:00 UTC). Thermistor locations at STA04 (WHOI), STA08 (MPL VLA1). Source, UD Tripod 1 (STA05), at 100 m depth with hydrophone array, UD Tripod II (STA07), at 108 m depth. The ray paths of interest in this paper are defined as follows: The direct (non-refracted) ray path and bottom bounce are shown in black, along with the downward refracted direct path and bottom bounce in green. Surface bounce rays are shown in dashed red and in yellow, a ray path is downward refracted beyond the range of the UDel Tripod II.

Fluctuations in the temperature profile are shown to influence ray path refraction and angular spread in the direct path reception over short periods of time. It is shown that in both measured data and PE modeled beamforming that the angular spread and intensity of the direct path signal in the lower water column is a function of isotherm depression and elevation (Figure 7). The steep slope of bathymetry shoreward and internal waves propagating towards the acoustic path from different source directions, are driving factors of isotherm oscillations over periods of 1 hour or less. The angular, temporal and spatial spread of the received signal are clearly functions of the water column temperature structure and correspondingly variations of the sound speed profile in the mid to lower water column.

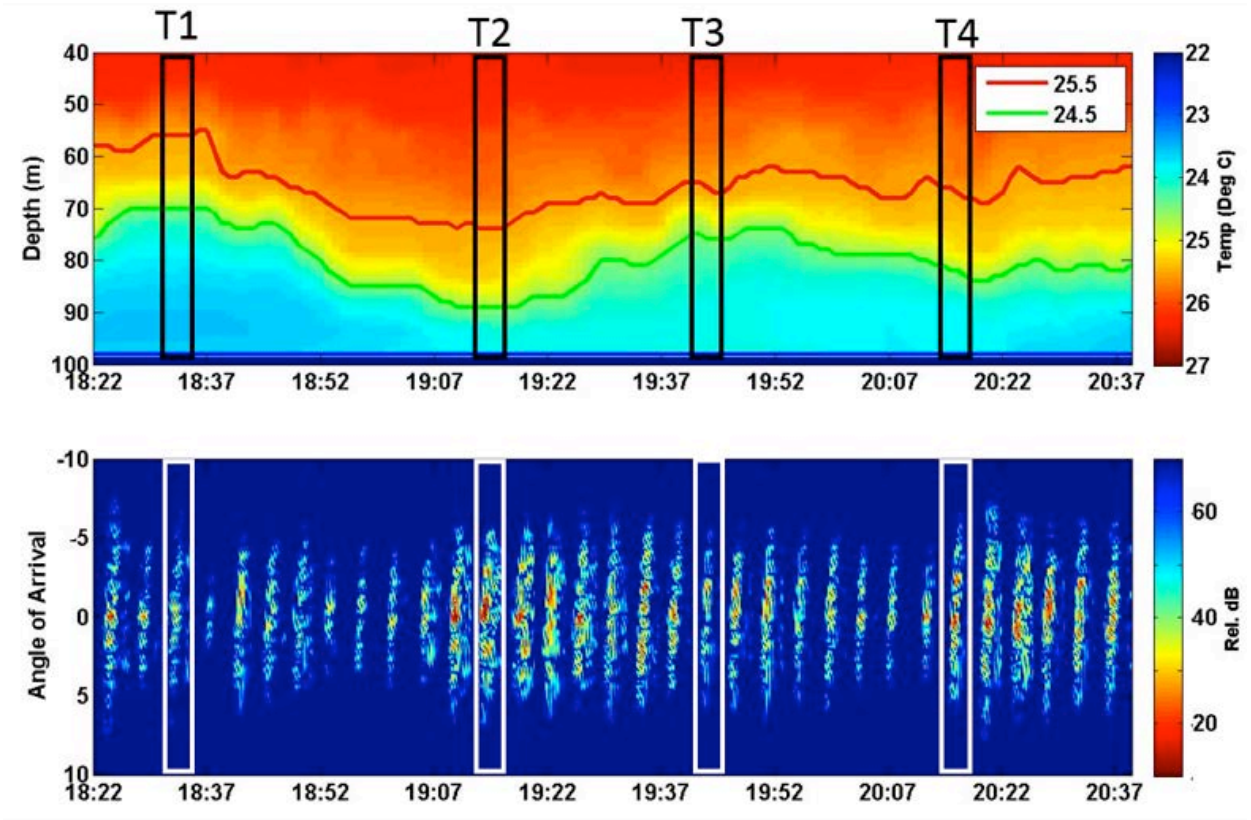

Figure 6. Vertical beamforming of measured impulse response across all array elements and application of Gaussian steering revealed strong correlation between vertical temperature profiles and angular spread of the direct path receptions.

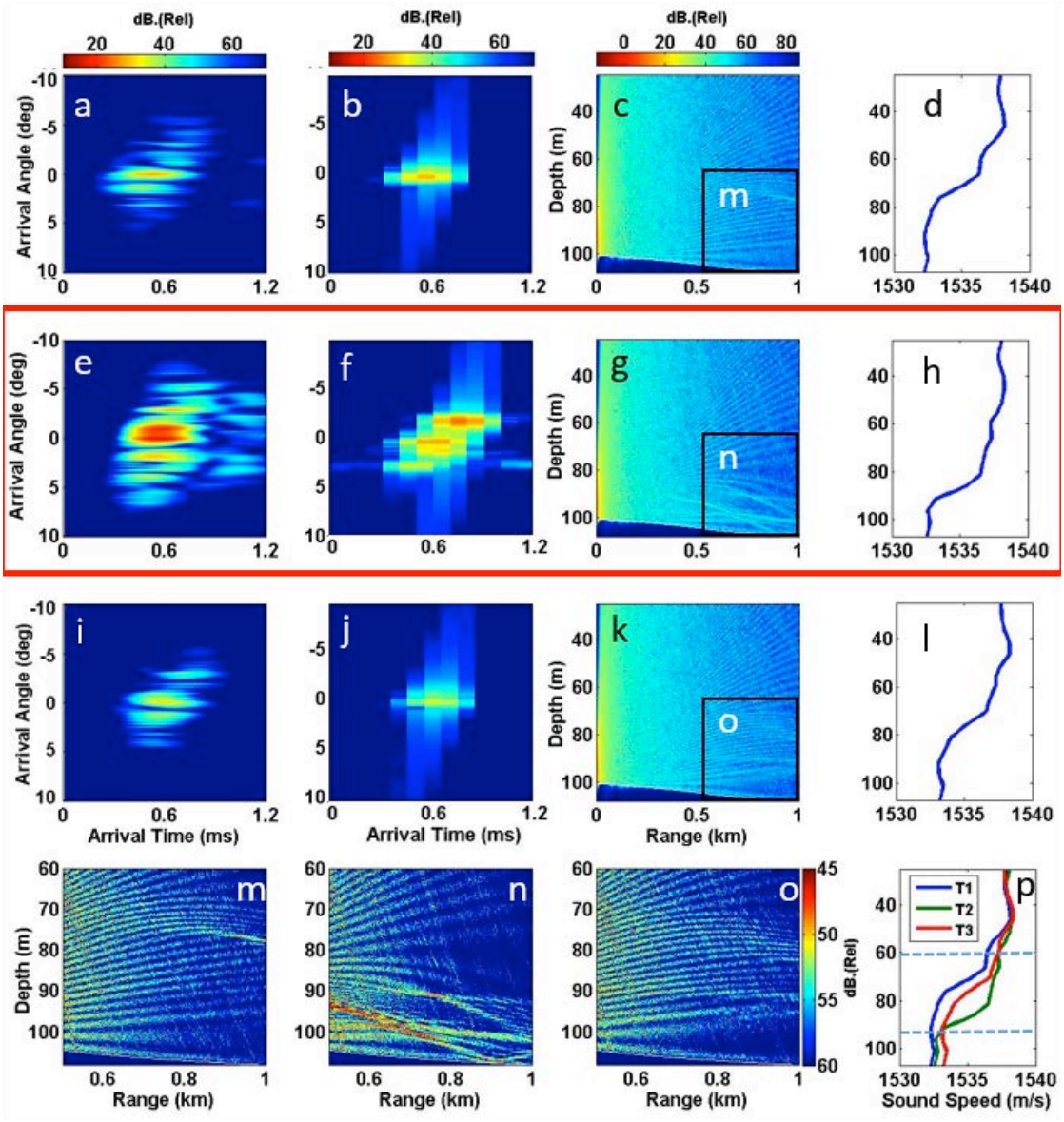

Figure 7. At T2 (19:15 UTC) in (e) the beamformed result shows separate regions of local maxima and minima intensity. The angular separation of regions of high and low intensity in the direct path signal is unique to the depressed isotherm structure at this time. The total angular spread in the data is 11°. The PE modeled result in (f) also has separate regions of varying intensity with a total angular spread of 10°. The PE acoustic field in (g) shows downward beam refraction below 85 m and strongest beam convergence between 92 and 108 m. In the measured SSP shown in Fig. 7(h) the highest gradient of sound speed begins at 85 m.

C. Design, Fabrication, and Test of Vertical Acoustic Line Array (VALA) for Sediment Characterization Experiment

The vertical acoustic line array (VALA), containing one 2-channel marine recorder with sampling frequency at 192 kHz from University of Delaware, one 4-channel SHRU from WHOI, ten RBR thermistors, one RBR depth sensor, two SBE37 TCP sensors, one SBE39 TP sensor, and one Star Oddi thermistor, was deployed at 18:16 UTC on 7/24/2015 and retrieved at 17:52 UTC on 7/30/2015 on the New England shelf (40.47738, -70.60397) of the United States in order to record environmental noise data in the region in addition to the acoustic signals generated by the combustive sound source (CSS) designed and operated by the ARL-UT [7] during the ONR-sponsored seabed characterization survey. The VALA array was designed in Ocean Acoustic Lab, University of Delaware. Calculations for designing and analyzing the VALA array were made using a software, 'Mooring Design and Dynamics (MDD)'. The array was designed and fabricated by Mr. Tim Deering (deering@udel.edu) at the Ship Operations department, the University of Delaware. The diagram of the mooring and the sensor location are shown in Fig. 8 and Table 1, respectively.

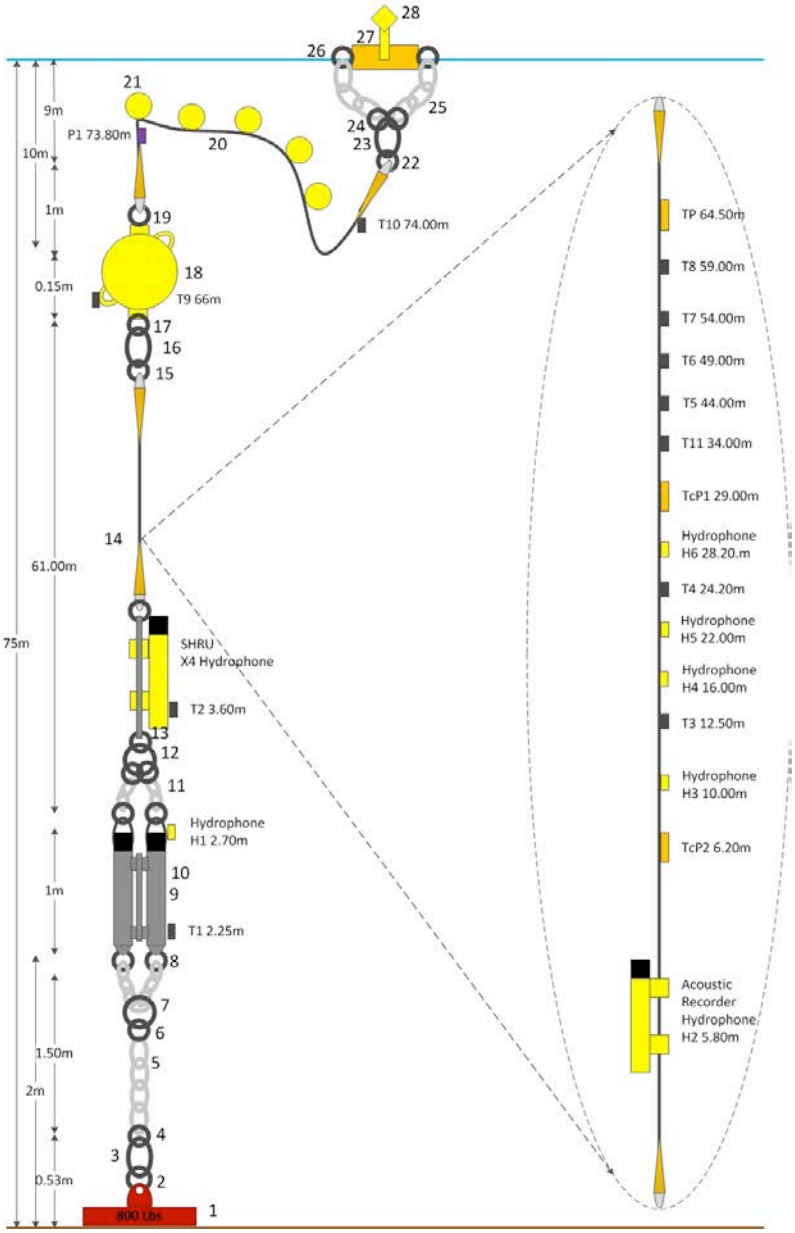

Figure 8. Mooring Configuration.

Table 1. Sensor location

SN	Name	H from anchor ring	Notes
100086	T1	2.25	On Acoustic Release
	H1	2.70	SHRU1
100091	T2	3.60	On SHRU body
	H2	5.80	UD 1
	TCP2	6.20	
	H3	10.00	SHRU2
100093	T3	12.50	
	H4	16.00	UD2
	H5	22.00	SHRU3
100089	T4	24.20	
	H6	28.20	SHRU4
	TCP1	29.00	
T-2088	T11	34.00	
100092	T5	44.00	
100087	T6	49.00	
100090	T7	54.00	
100095	T8	59.00	
	TP	64.50	
100096	T9	66.00	On sub-surface buoy
78504	P1	73.80	
100094	T10	74.00	

In Fig. 9, subplot (a) shows the time series signature of CSS received by the source monitoring hydrophone. (b) and (c) are the results recorded by the UDEL two-channel marine recorder on the VALA at depths of 59 m and 69.2 m, respectively. The high sampling rate (192 kHz) enables us to record the high frequency data. (d) and (e) are their corresponding time-frequency plots. (f) shows the bottom layer structure along the sound propagation track obtained by John Goff [8]. For the short-range propagation (2.2 km), the received signal contains high frequency components. CSS1 is up to about 7 kHz.

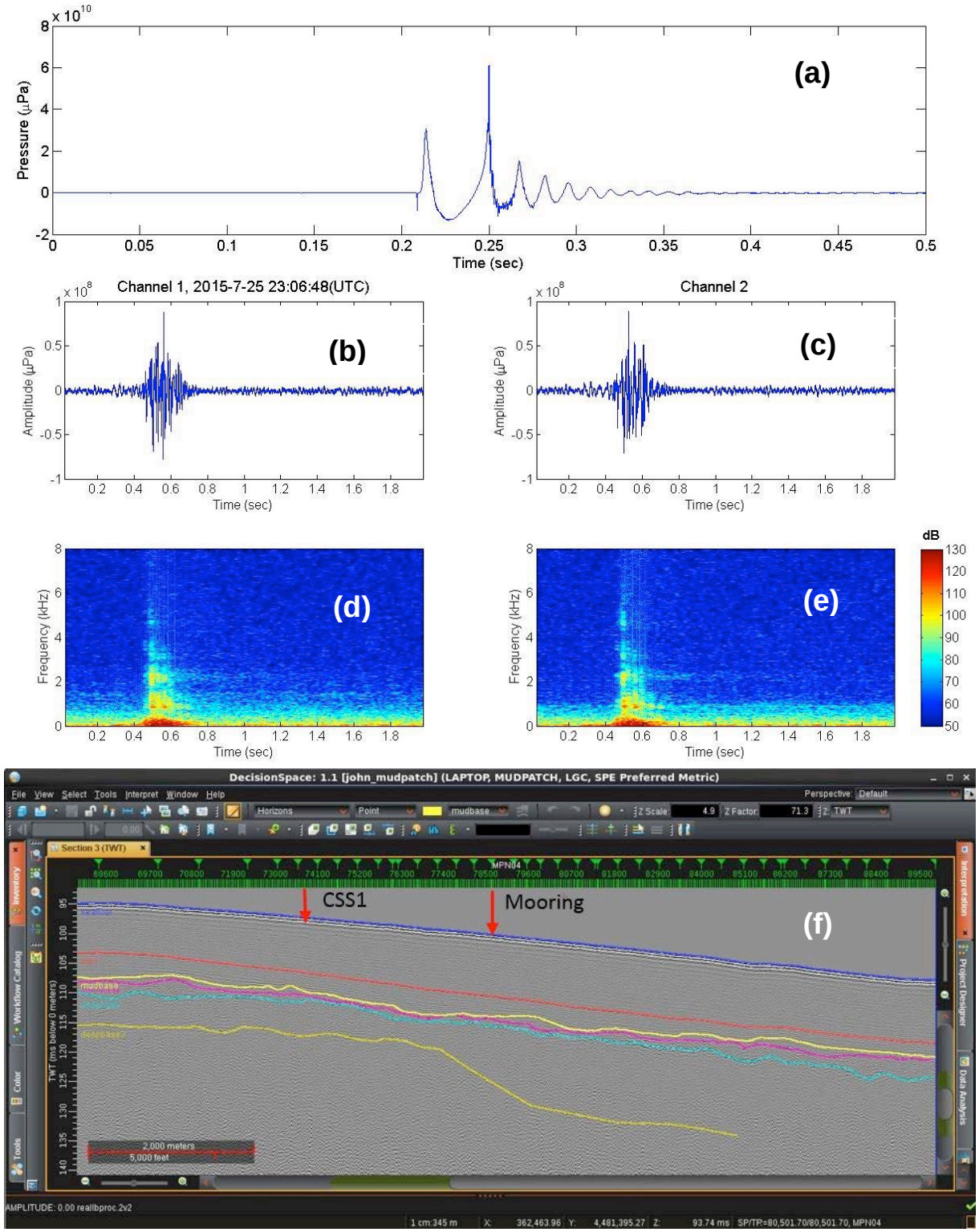

Figure 9. CSS1 (SD=5m, Range=2.2km) [Applied Research Lab.- UT] received by Univ. of Delaware marine recorder (2 channels). Sediment cross section plot courtesy of J. Goff [8].

Ocean ambient noise, including anthropogenic noise from ships and nature noise from marine mammals and wind forces, are expected around the SCE experimental site. In order to obtain the ambient noise information. The ambient noise measurement by VALA was performed for about 6 days. Figs. 10 and 11 show the average power spectrum density plots obtained by analyzing 10-second acoustic data every 5 minutes during the 6-day measurement. Fig. 10 is the low frequency (0 - 200 Hz) result from the lower channel of UDEL marine recorder at depth of 69.2 m. Figure 11 shows the result with frequency up to 9000 Hz.

In the low frequency plot (Fig. 10), we can see the low frequency ambient noise feature, e. g. noises from the passing ships, strumming noise at 5 and 20 Hz, etc. In the Fig. 11, chirp signals from R/V Sharp were recorded. Whistles and clicks by dolphin are also observed. In addition, there was one type of unknown sound with frequency up to 2.5 kHz. These sound started every midnight (UTC) and lasted about 9.5 hours.

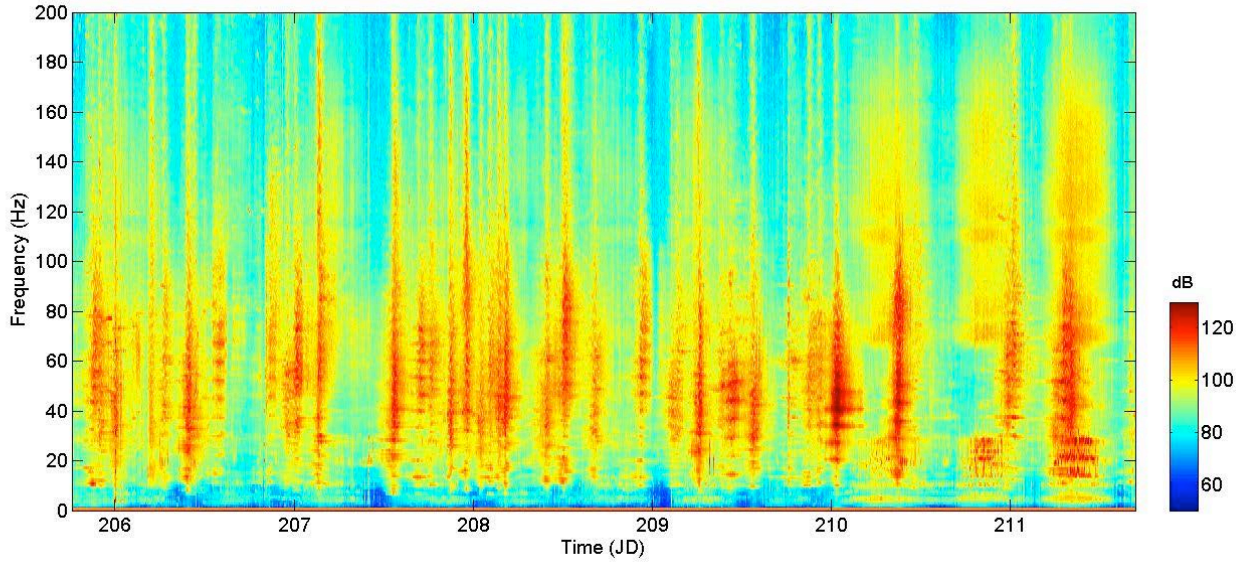

Fig 10. Low frequency ambient noise measurements.

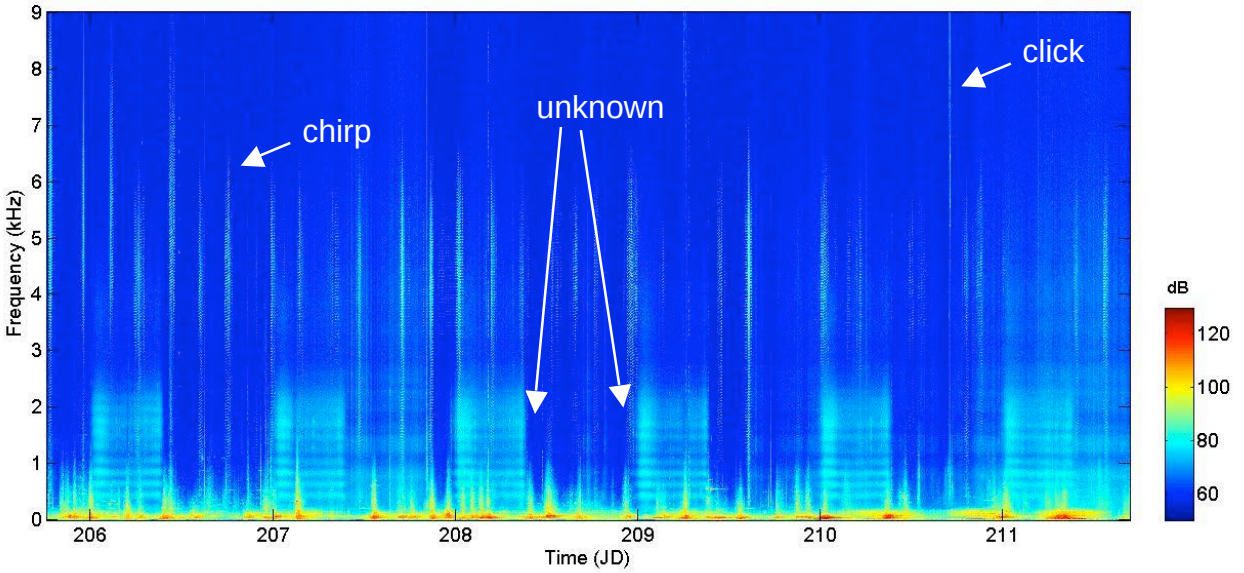

Fig 11. Ambient noise measurements up to 9 kHz. Chirp signals and dolphin sound were observed. Unknown sound with frequency up to 2.5 kHz was also recorded.

Figure 12 shows the measured temperature profile as a function of geo-time by interpolating the data from nine RBR thermistors mounted on the VALA. The times when we have CTD cast and CSS deployments are marked by black and red dashed dotted lines, respectively. Strong internal wave events were observed.

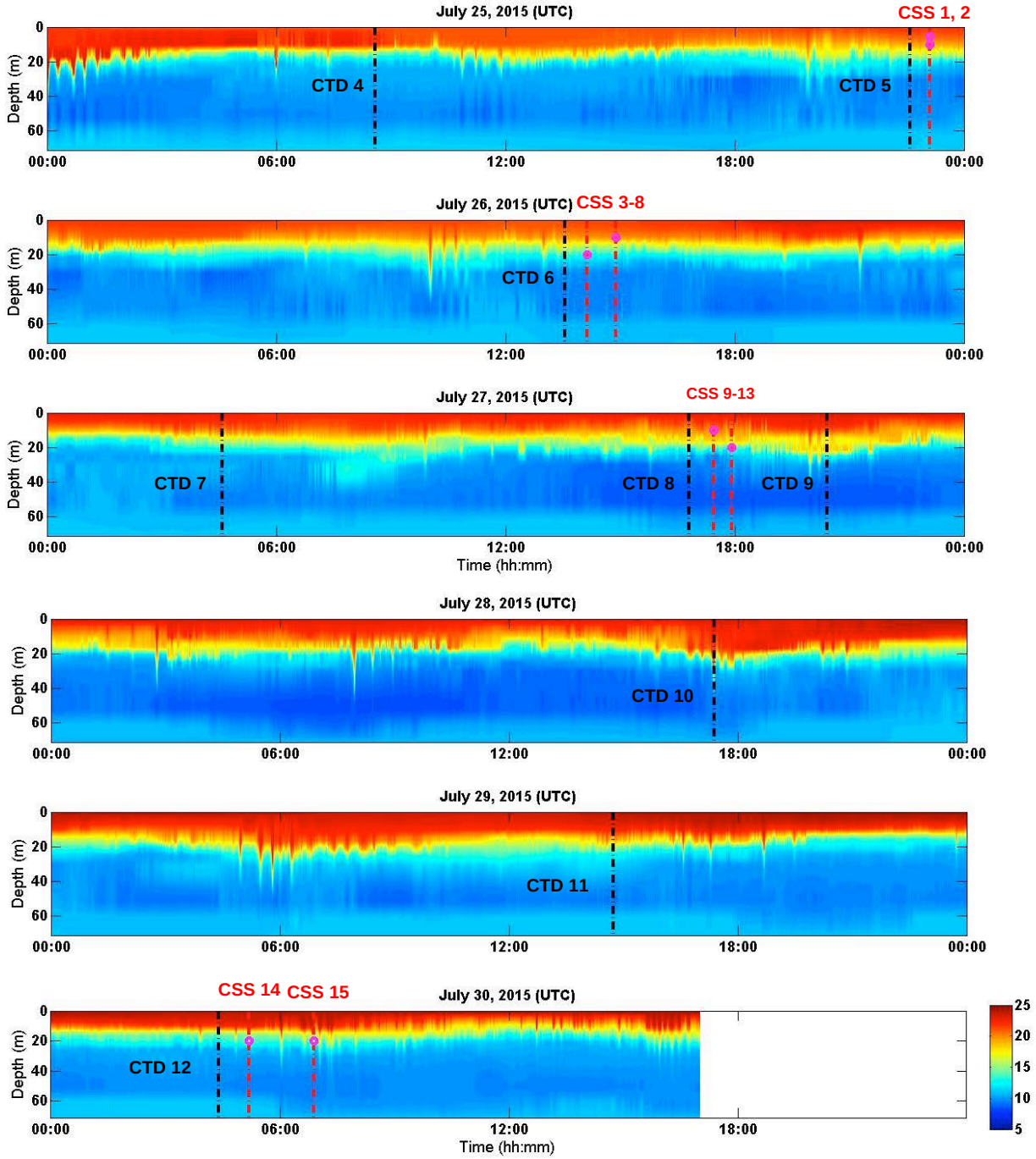

Fig. 12. Water column temperature profile at VALA.

IMPACT/APPLICATIONS

The low frequency component of our research contributes to the understanding of acoustic propagation in complex shallow water regions. We have developed a model that is able to reproduce the mechanism of acoustic intensity variation due to internal waves and to quantitatively predicts the time and location of specific details. The spatial and temporal coherence of individual normal mode obtained before, onset, and after the IW events have been studied. The high frequency part of our research has contributed to the understanding of the effects of surface wave roughness and directionality as well as bubble effects on sound propagation, which in turn affect the performance of acoustic communication signals.

RELATED PROJECTS

During this year we have collaborated on a related MURI project [N00014-11-1-0701] (PI: T. Duda]. In addition, we have worked on the Arctic Shallow Water Acoustic Research with D. Knobles (ARL-UT), and P. Worcester (SIO).

REFERENCES

[1] W.S.Hodgkiss, et al.,"Kauai Acomms MURI 2008 (KAM08) Experiment Trip Report," 2008.

[2] W. S. Hodgkiss, et al., "Kauai Acomms MURI 2011 (KAM11) Experiment Trip Report,"2011.

[3] M. Badiey, L. Wan, and A. Song, "Three-dimensional mapping of evolving internal waves during the Shallow Water 2006 experiment," J. Acoust. Soc. Am., 134(1), EL7-EL13, 2013.

[4] E. A. Karjadi, M. Badiey, J. T. Kirby, and C. Bayindir, "Effects of surface gravity waves on high-frequency propagation in shallow water," IEEE J. Ocean. Eng. 37, 112-121 (2012).

[5] J. Senne, "High Frequency Acoustic Propagation under Variable Sea Surfaces," Ph.D. Dissertation, University of Delaware, Newark, Delaware, 2012.

[6] L. Wan, M. Badiey, and J. F. Lynch,, (2013) "Acoustic normal mode fluctuations due to internal waves in the Shallow Water 2006 experiment." J. Acoust. Soc. Am., 134(5):4036.

[7] A. R. McNeese, P. S. Wilson, J. D. Sagers, and D. P. Knobles, (2014) "An impulsive source with variable output and stable bandwidth for underwater acoustic experiments",J.Acoust.Soc.Am.136

[8] Goff, J., Personal communication, July, 2015.

PUBLICATIONS

[1] M. Badiey, A. Muenchow, L. Wan, M. S. Ballard, D. P. Knobles and J. D. Sagers, "Modeling three dimensional environment and broadband acoustic propagation in Arctic shelf-basin region (A)", The Journal of the Acoustical Society of America, Volume 136, p. 2317, (2014)

[2] M. Badiey, J. E. Eickmeir, and A. Song, (2014) "Arrival-time fluctuations of coherent reflections from surface gravity water waves," J. Acoust. Soc. Am., 135, EL226.

[3] L. Wan and M. Badiey, "Coherence measurements of acoustic normal modes during one month of internal wave events on the New Jersey continental shelf (A)", The Journal of the Acoustical Society of America, Volume 135, p. 2305, (2014)

[4] L. Wan and M. Badiey, "Horizontal coherence of sound propagation in the presence of internal waves on the New Jersey continental shelf (A)", The Journal of the Acoustical Society of America, Volume 137, p. 2390, (2015)

[5] L. Wan and M. Badiey, "Seabed attenuation inversion from broadband reverberation measurements in the Yellow Sea (A)", The Journal of the Acoustical Society of America, Volume 137, p. 2283, (2015)